Hindawi
Journal of Nanomaterials
Volume 2022, Article ID 2891315, 13 pages
https://doi.org/10.1155/2022/2891315

Research Article

Melting Heat Transition in a Spinning Flow of Silver-Magnesium Oxide/Engine Oil Hybrid Nanofluid Using Parametric Estimation

Muhammad Bilal,[1] Taza Gul ,[1] Abir Mouldi,[2] Safyan Mukhtar,[3] Wajdi Alghamdi ,[4] Souhail Mohamed Bouzgarrou,[5] and Nosheen Feroz[6]

[1]*Department of Mathematics, City University of Science and Information Technology, Peshawar 25000, Pakistan*
[2]*Department of Industrial Engineering, College of Engineering, King Khalid University, Abha 61421, Saudi Arabia*
[3]*Department of Basic Sciences, Deanship of Preparatory Year, King Faisal University, Hafuf, Al Ahsa, Saudi Arabia*
[4]*Department of Information Technology, Faculty of Computing and Information Technology, King Abdulaziz University, Jeddah 80261, Saudi Arabia*
[5]*Department of Civil Engineering, Faculty of Engineering, Jazan University, Saudi Arabia*
[6]*Department of Mathematics, Bacha Khan University Charsadda, KP, Pakistan*

Correspondence should be addressed to Taza Gul; tazagul@cusit.edu.pk

Received 7 November 2021; Revised 8 May 2022; Accepted 20 May 2022; Published 15 June 2022

Academic Editor: P. Davide Cozzoli

This study reports the three-dimensional (3D) flow of Ag-MgO hybrid nanofluid (HNF) over a spinning disc of flexible thickness in the presence of modified Fourier law. The HNF is contained of silver and magnetic nanoparticulate in the base fluid engine oil. The energy transition has been examined in the involvement of melting heat propagation. The highly nonlinear system of partial differential equations (PDEs) is processed by adopting the proper similarity conversions to attain the coupled ODE system. The obtained system of modeled equations is numerically solved by employing the Parametric Continuation Method (PCM). The nature of various constraints, as opposed to the velocities, energy, and mass transmission, is portrayed and described. In comparison to the simple nanofluid flow, the hybrid nanoliquid flow's velocity and heat conduction are observed to have a significant influence. As a result, the functionality of the hybrid nanoliquid is significantly superior to that of the conventional nanofluid. The positive variation in power-law exponent n and Reynold number Re significantly enhances the fluid velocity. The effect of both melting coefficient and thermal relaxation term reduces fluid temperature.

1. Introduction

In the analysis of HNF due to its substantial participation in engineering constraints and modern machinery, the examination of HNF flow over a turning disk with energy communication has taken significant interest [1, 2]. The well-recognized uses consist of electric control techniques, cocircling apparatus, aerodynamic systems, whirling machines, biochemical reactions, supercomputer management, and hydrothermal sectors [3]. Lv et al. [4] investigated the effects of magnetism and Hall potential on nanofluid flow across a revolving disc. Their target was to increase the level of heat dissipation for technological reasons. As per the conclusions, the modification of CNTs in water is substantially more favorable than that of other nanoparticles due to their C–C interaction. Li et al. [5] employed the bvp4c packages to perform a percentage approximation for Darcy HNF flow over a pierced rotation disc with heat slip. Khan et al. [6] investigated the chemical reaction that influences Maxwell fluid flow over a diagonally gyrating oscillating disc with the magnetic flux during unstable motion. It should be observed that the energy transference ratio raises drastically when the disc radiation and rotation factors increase. The unsteady slip flow with entropy production over a revolving disc under the action of a ferromagnetic material was studied by Shuaib et al. [7] and Bilal et al. [8]. The slip factor seems to be effective in regulating flow and heat characteristics. The Oldroyd-B fluid flow was investigated by Hafeez et al. [9] using a whirling disc. As the relaxation time factor is increased, the flow rate is spotted to diminish. The fluid potential spectrum is also lowered as the thermal relaxation phase develops. HNF flow through a swaying disc with sessile microbes and chemical reactions was discovered by Waqas et al. [10]. A concordance with previous research and a full simple geometric presentation for key variables aid the presented rebuttal. Tassaddiq et al. [11] created an HNF flow over an indefinite impermeable rotating disc. The role of magnetic flux was used to accurately analyze the positive rotation of nanofluid flow. Their primary project purpose was to raise public awareness about energy usage in scientific and technological contexts. The addition of ferric oxide Fe3O4 nanoparticles enhances the heat transition rate considerably [12].

Nanofluids are a new type of solution that operates efficiently in heat exchanger when compared to traditional fluids. When the thermal sensitivity is high enough, nanocomposite can be used in a wide range of thermal processes, including freezing [13–17]. Nanofluid flow is used in a variety of applications, including heat converters, geothermal energy, heat pumps, metallurgy, climate control, the automobile sector, turbines, microelectronics, nuclear condenser networks, ships, medicine, and circuit condensation [18–21]. The vast demand for thermal energy in the era of development of science and technology cannot be met with widely utilized fluids. When similar base liquids were produced with the addition of tiny-sized particles, however, a substantial improvement in thermal properties was seen [22]. In the present analysis, we have utilized the MgO (magnesium oxide) and Ag (silver) nanomaterials in the base fluid. MgO is a chemical made up of Mg^{2+} and O^{2-} ions at 700–1500°C [23]. For metallurgical and electronic operations, MgO is more practical [24]. Similarly, Ag nanoparticulates' might be exploited to control bacterial movement in an array of products, involving dental work, injuries and wound therapy, surgery, and biomedical apparatus [25, 26]. Ahmadian et al. [27] investigate a 3D simulation of an unstable Ag-MgO HNF flow with heat conduction induced by a curvy spinning disc going up and downwards. With the dispersion of Ag-MgO nanocrystals, the HNF is created. The issue was solved using the PCM technique. The usage of Ag-MgO is thought to be more effective in overcoming poor energy transfer. Among metal and metal oxide, silver and magnesium oxide nanoparticles have been widely recorded to have broad-spectrum antibiotic assets [28]. Silver nanoparticles are the most widely utilized inorganic nanoparticles, having several applications in biomaterial detection and antibacterial activities [29]. Anuar et al. [30] used Ag and MgO nanocrystals in water to evaluate the energy distribution of a hybrid nanoliquid through an extending sheet with suction and buoyant force effects. The findings show that improving the quantity of Ag nanoparticles in HNF lowers the energy transference. Gangadhar et al. [31] arithmetically addressed the heat transport properties of a hybrid nanofluid mixture combining Au and MgO nanoparticulate. Hiba et al. [32] evaluated the thermal performance of HNF including magnesium oxide and Silver and across a highly permeable hollow microplate under magnetic impact. Recently, several researchers have been reported on the study of hybrid nanofluid flow [33–36].

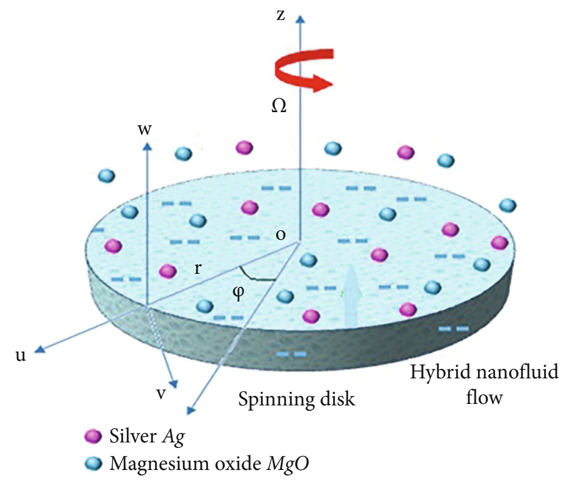

Figure 1: Spinning disk geometry.

PCM tackles a lot of challenging nonlinear boundary value problems that other numerical techniques cannot solve. Convergence is subject to the relaxation variables and initial strategy for many problems that are generally addressed by traditional computational approaches [37–40]. The PCM's goal is to determine that the proposed methodology can be used to solve complex nonlinear problems related to industry [41]. Shuaib et al. [42] emphasized the 3D oscillating fluid and energy conductivity across the surface of an irregular elastic revolving disc. The fluid flow has been examined in the context of an external magnetism flux. The phenomena of an ionic fluid flow throughout a spinning disc were discovered by Shuaib et al. [43]. The Poisson's and Planck models were used to computing the molecular interactions. Dombovari et al. [44] investigated the robustness of nonlinear hydrological systems using a parametric continuation technique. They also looked into static bifurcation, which arises while addressing complex initial value systems with distinctive roots, and devised a method for efficiently determining the points of bifurcation. Ref. [45, 46] may be used to solve the stated challenge in the future.

The assessment was aimed at reporting the 3D flow of Ag- and MgO-based HNF over a spinning disk of flexible thickness. The HNF is synthesized with the composition of silver and magnetic nanomaterials in the engine oil. The energy transition is examined with the involvement of melting heat propagation. To evaluate the behaviors of the fluid flow, Tiwari and Das's model is employed. The nonlinear system of PDEs is processed through the proper similarity conversions to attain the coupled ODE system. The obtained system of modeled equations is numerically solved employing the Parametric Continuation Method (PCM). In the next section, the formulation, solution methodology, and results and discussion have been discussed in detail.

2. Mathematical Formulation

In this study, we considered the steady and incompressible flow of Ag-MgO hybrid nanoliquid over a gyrating disk of variable thickness $z = a(1 + r^*)^{-m}$, moving with fixed angular velocity Ω about the z-axis. Here, u, v, and w are the velocity component along r, θ, z direction, respectively. T_∞ is the free stream temperature, and T_m is the temperature of the melting surface. Figure 1 reveals the flow mechanism over a spinning disk. The modeled equations can be rebound as [47–49]

$$\frac{\partial u}{\partial r} + \frac{u}{r} + \frac{\partial w}{\partial z} = 0, \tag{1}$$

$$u\frac{\partial u}{\partial r} + v\frac{\partial u}{\partial z} = \nu_{hnf}\frac{\partial^2 u}{\partial z^2} + \frac{v^2}{r} - \sigma_{hnf}B_0^2 u, \tag{2}$$

$$u\frac{\partial v}{\partial r} + w\frac{\partial v}{\partial z} = \nu_{hnf}\frac{\partial^2 v}{\partial z^2} - \frac{uv}{r} - \sigma_{hnf}B_0^2 v, \tag{3}$$

$$\begin{aligned} u\frac{\partial T}{\partial r} + w\frac{\partial T}{\partial z} &= \frac{k_{hnf}}{(\rho C_p)_{hnf}}\frac{\partial^2 T}{\partial z^2} - \lambda \\ &\cdot \begin{pmatrix} u^2\dfrac{\partial^2 T}{\partial r^2} - w^2\dfrac{\partial^2 T}{\partial z^2} + \left(u\dfrac{\partial u}{\partial r}\dfrac{\partial T}{\partial r} + w\dfrac{\partial u}{\partial z}\dfrac{\partial T}{\partial r}\right), \\ +2uw\dfrac{\partial^2 T}{\partial r\partial z} + \dfrac{\partial T}{\partial z}u\left(\dfrac{\partial w}{\partial r} + w\dfrac{\partial w}{\partial z}\right), \end{pmatrix} \end{aligned} \tag{4}$$

$$u\frac{\partial C}{\partial r} + v\frac{\partial C}{\partial z} = D_{hnf}\frac{\partial^2 C}{\partial z^2} - k(C - C_0). \tag{5}$$

Here, (u, v, w) exhibit the velocity element, and ν_{hnf}, k_{hnf} and $(\rho C_p)_{hnf}$ reveal the kinematic viscosity, thermal conductivity, and volumetric heat capacity, respectively.

The boundary conditions are

$$\begin{aligned} &u = 0, w = 0, v = r\Omega, T = T_\infty, C = C_\infty \text{at } z = 0, \\ &k_{hnf}\left(\frac{\partial T}{\partial z}\right)_{z=a(1-r^*)^{-m}} \\ &\quad = \rho_{hnf}(\lambda^* + C_s(T_m - T_0))w(r, z), \\ &u \longrightarrow 0, v \longrightarrow 0, T \longrightarrow T_\infty, \\ &\quad C \longrightarrow C_\infty \text{when } z \longrightarrow \infty. \end{aligned} \tag{6}$$

Table 1 shows the thermophysical properties of nanofluids and hybrid nanofluids in terms of viscosity, density, heat capacity and thermal conductivity.

Incorporating the following transformation in Equations (1)–(5) and (6)

$$\begin{aligned} &u = \Omega r F(\eta), v = \Omega r G(\eta), w = \frac{-R_0\Omega(1 + r^*)^{-m}}{\left(R_0^2\Omega\rho_f/\mu_f\right)^{1/n+1}}J(\eta), \theta(\eta) \\ &= \frac{T - T_m}{T_\infty - T_m}, \phi(\eta) = \frac{C - C_m}{C_\infty - C_m}, \\ &\eta = \frac{z}{R_0}(1 + r^*)^{-m}\left(\frac{R_0^2\Omega\rho_f}{\mu_f}\right)^{1/n+1}, \end{aligned} \tag{7}$$

we get

$$J'(\eta) + 2F(\eta) + \eta m\varepsilon F'(\eta) = 0, \tag{8}$$

$$\begin{aligned} &\left(\frac{\mu_{hnf}}{\mu_f}\right)\mathrm{Re}^{1-n/1+n}(1 + r^*)^{2m}F''(\eta) + \left(\frac{\rho_{hnf}}{\rho_f}\right) \\ &\cdot \left[-F^2(\eta) - J(\eta)F'(\eta) + G^2(\eta) - \eta\varepsilon m F(\eta)F'(\eta)\right] = 0, \end{aligned} \tag{9}$$

$$\begin{aligned} &\left(\frac{\mu_{hnf}}{\mu_f}\right)\mathrm{Re}^{1-n/1+n}(1 + r^*)^{2m}G''(\eta) + \left(\frac{\rho_{hnf}}{\rho_f}\right) \\ &\cdot \left[-2G(\eta)F(\eta) - J(\eta)G'(\eta) - \eta m\varepsilon F(\eta)G'(\eta)\right] = 0, \end{aligned} \tag{10}$$

$$\begin{aligned} &\left(\frac{k_{hnf}}{k_f}\right)\left(\frac{\mathrm{Re}^{1-n/1+n}(1 + r^*)^{2m}}{\mathrm{Pr}}\right)\theta''(\eta) - \gamma\left(\frac{(\rho C_p)_{hnf}}{(\rho C_p)_f}\right) \\ &\cdot \begin{bmatrix} m(m-1)\eta\varepsilon^2 F^2(\eta)\theta'(\eta) + \eta^2 m^2\varepsilon^2 F(\eta)\theta''(\eta) \\ +J^2(\eta)\theta''(\eta) + \eta m\varepsilon F^2(\eta)\theta'(\eta) \\ +\eta^2 m^2\varepsilon^2 F(\eta)F'(\eta)\theta'(\eta) + \eta m\varepsilon\theta'(\eta)J(\eta)F'(\eta) \\ +\eta m\varepsilon\theta'(\eta)J'(\eta)F(\eta) + J(\eta)J'(\eta)\theta(\eta) \end{bmatrix} \\ &- \eta m\varepsilon\theta'(\eta)F(\eta) - J(\eta)\theta'(\eta) = 0, \end{aligned} \tag{11}$$

$$\begin{aligned} &\varphi''(\eta)\alpha^2(1 + r^*)^{-2m} - \frac{1}{Sc}d_1\varphi(\eta) \\ &+ \frac{1}{Sc}ma\varepsilon\eta(R_0 + 1)F(\eta)\varphi(\eta) \\ &- \frac{1}{Sc}(1 + r^*)^{-m}aG(\eta)\varphi(\eta) = 0. \end{aligned} \tag{12}$$

Table 1: The thermophysical properties of hybrid nanofluid and model [47].

	$\phi_{nf} = \left(\phi_{MgO} \text{ or } \phi_{Ag}\right)$	$\phi_{hnf} = \left(\phi_{MgO} + \phi_{Ag}\right)$
Viscosity μ	$\mu_f/(1-\phi_{Au})$ $\mu_f/\left(1-\phi_{Ag}\right)$	$\mu_f/\left(1-\phi_{hnf}\right)^{2.5}$
Density ρ	$(1-\phi_{Au})_{\rho f} + \phi_{Au}\rho_{Au}$ $\left(1-\phi_{Ag}\right)_{\rho f} + \phi_{Ag}\rho_{Ag}$	$\left(1-\phi_{hnf}\right)\rho_f + \phi_{MgO}\rho_{MgO} + \phi_{Ag}\rho_{Ag}$
Heat capacity $\left(\rho C_p\right)$	$(1-\phi_{Au})\left(\rho C_p\right)_f + \phi_{Au}\left(\rho C_p\right)_{Au}$ $\left(1-\phi_{Ag}\right)\left(\rho C_p\right)_f + \phi_{Ag}\left(\rho C_p\right)_{Ag}$	$\left(1-\phi_{hnf}\right)\left(\rho C_p\right)_f + \phi_{MgO}\left(\rho C_p\right)_{MgO} + \phi_{Ag}\left(\rho C_p\right)_{Ag}$
Thermal conductivity k	$\left(k_{Au} + 2k_f - 2\phi_{Au}\left(k_f - k_{Au}\right)/k_{Au} + 2k_f + 2\phi_{Au}\left(k_f - k_{Au}\right)\right)k_f$ $\left(k_{Ag} + 2k_f - 2\phi_{Ag}\left(k_f - k_{Ag}\right)/k_{Ag} + 2k_f + 2\phi_{Ag}\left(k_f - k_{Ag}\right)\right)k_f$	$k_{Ag} + 2k_{nf} - 2\phi_{Ag}\left(k_{nf} - k_{Ag}\right)/k_{Ag} + 2k_{nf} + 2\phi_{Ag}\left(k_{nf} - k_{Ag}\right)$ $\times\left(k_{MgO} + 2k_f - 2\phi_{MgO}\left(k_f - k_{MgO}\right)/k_{MgO} + 2k_f + 2\phi_{MgO}\left(k_f - k_{MgO}\right)\right)k_f$
Diffusivity α	$k_{nf}/\left(\rho C_p\right)_{nf}$	$k_{hnf}/\left(\rho C_p\right)_{hnf}$

The transform conditions are

$$F(\alpha)=0, G(\alpha)=1, \frac{k_{hnf}}{k_f}\mathrm{Me}\,\mathrm{Re}^{1-n/1+n}(1+r^*)^{2m}\theta'(\alpha) + \frac{\rho_{hnf}}{\rho_f}\Pr J(\alpha)=0, \theta(\alpha)=1, \varphi(\alpha)=1,$$
$$F(\infty)=0, \theta(\infty)=0, \varphi(\infty)=0, G(\infty)=0. \tag{13}$$

Here, α is the disk thickness coefficient, Re is the Reynold number, Me is the melting constant, ε is the constant coefficient, r^* is the dimensionless radius parameter, γ is the thermal relaxation parameter, and Pr is the Prandtl number defined as [47]

$$\alpha=\frac{a}{R_0}\left(\frac{R_0^2\Omega\rho_f}{\mu_f}\right)^{1/n+1}, \mathrm{Re}=\frac{R_0^2\Omega\rho_f}{\mu_f},$$
$$\mathrm{Me}=\frac{(T_\infty-T_m)C_p}{C_s(T_m-T_0)+\lambda^*}, \varepsilon=\frac{r}{R_0+r}, \tag{14}$$
$$r^*=\frac{r}{R_0}, \gamma=\Omega\lambda, \Pr=\frac{\mu_f(C_p)_{nf}}{k_f},$$

where F, G, and J denote the radial, tangential, and axial velocities, and ϕ, θ show the dimensionless concentration and temperature. The deformations are expressed as

$$\begin{aligned} f(\xi)&=f(\eta-\alpha)=F(\eta),\\ j(\xi)&=j(\eta-\alpha)=J(\eta),\\ g(\xi)&=g(\eta-\alpha)=G(\eta),\\ \theta(\xi)&=\theta(\eta-\alpha)=\theta(\eta),\\ \varphi(\xi)&=\varphi(\eta-\alpha)=\varphi(\eta). \end{aligned} \tag{15}$$

Using Equation (15), Equations (7)–(12) take the form

$$J'(\xi)+\xi m\varepsilon f'(\xi)+\alpha m\varepsilon f'(\xi)+2f(\xi)=0, \tag{16}$$

$$\left(\frac{\mu_{hnf}}{\mu_f}\right)\mathrm{Re}^{1-n/1+n}(1+r^*)^{2m}f''(\xi)+\left(\frac{\rho_{hnf}}{\rho_f}\right)\cdot\begin{bmatrix}-f^2(\xi)-j(\xi)f'(\xi)-\xi m\varepsilon f(\xi)f'(\xi)\\ +g^2(\xi)-\alpha m\varepsilon f(\xi)f'(\xi)\end{bmatrix}=0, \tag{17}$$

$$\left(\frac{\mu_{hnf}}{\mu_f}\right)\mathrm{Re}^{1-n/1+n}(1+r^*)^{2m}g''(\xi)+\left(\frac{\rho_{hnf}}{\rho_f}\right)\cdot\begin{bmatrix}-j(\xi)g'(\xi)-\xi m\varepsilon f(\xi)g'(\xi)\\ -2g(\xi)f(\xi)-\alpha m\varepsilon f(\xi)g'(\xi)\end{bmatrix}=0, \tag{18}$$

$$\left(\frac{k_{hnf}}{k_f}\right)\left(\frac{\mathrm{Re}^{1-n/1+n}(1+r^*)^{2m}}{\Pr}\right)\theta''(\xi) - (\xi+\alpha)m\varepsilon f(\xi)\theta'(\xi)-j(\xi)\theta'(\xi)-\gamma\left(\frac{(\rho C_p)_{hnf}}{(\rho C_p)_f}\right)\cdot\begin{bmatrix} m(m-1)(\xi+\alpha)\varepsilon^2 f^2(\xi)\theta'(\xi)+(\xi+\alpha)^2 f(\xi)\theta''(\xi)\\ +j^2(\xi)\theta''(\xi)+(\alpha+\xi)\varepsilon m f^2(\xi)\theta'(\xi)\\ +(\xi+\alpha)^2 m^2\varepsilon^2 f^2(\xi)f'(\xi)\theta(\xi)+(\xi+\alpha)m\varepsilon j(\xi)f'(\xi)\theta'(\xi)\\ +(\xi+\alpha)m\varepsilon j'(\xi)f(\xi)\theta'(\xi)+j(\xi)j'(\xi)\theta(\xi)\end{bmatrix}, \tag{19}$$

$$\begin{aligned}&\varphi''(\xi)\alpha^2(1+r^*)^{-2m}-\frac{1}{Sc}d_1\varphi(\xi)\\ &+\frac{1}{Sc}ma\varepsilon\xi(R_0+1)f(\xi)\varphi(\xi)\\ &+\frac{1}{Sc}ma^2\varepsilon(R_0+1)f(\xi)\varphi(\xi)\\ &-\frac{1}{Sc}(1+r^*)^{-m}ag(\xi)\varphi(\xi)=0,\end{aligned} \tag{20}$$

$$f(0)=0, g(0)=1, \theta(0)=1, \varphi(0)=1,$$
$$\frac{k_{hnf}}{k_f}\mathrm{Me}\,\mathrm{Re}^{1-n/1+n}(1+r^*)^{2m}\theta'(0)+\frac{\rho_{hnf}}{\rho_f}\Pr j(0)=0,$$
$$f(\infty)=0, g(\infty)=0, \theta(\infty)=0, \varphi(\infty)=0. \tag{21}$$

The skin friction is stated as

$$C_{fr}=\frac{\tau_{wr}}{\rho_f(R_0\Omega)^2}, C_{f\theta}=\frac{\tau_{w\theta}}{\rho_f(R_0\Omega)^2}. \tag{22}$$

Shear forces are

$$\tau_{wr}=\mu_{hnf}\left.\frac{\partial u}{\partial z}\right|_{z=(1+r^*)^{-m}}, \tau_{w\theta}=\mu_{hnf}\left.\frac{\partial v}{\partial z}\right|_{z=(1+r^*)^{-m}}. \tag{23}$$

The nondimensional form is

$$\mathrm{Re}^{n/n+1}C_{fr}=\left[\frac{\mu_{hnf}}{\mu_f}(1+r^*)^m\right]r^*f'(0), \mathrm{Re}^{n/n+1}C_{f\theta}=\left[\frac{\mu_{hnf}}{\mu_f}(1+r^*)^m\right]r^*g'(0). \tag{24}$$

3. Numerical Solution

The basic steps of PCM are as follows:Step 1: simplifying Equations (16)–(20) to 1st order with the boundary conditions

$$
\begin{gathered}
\chi_1 = f(\xi), \chi_2 = f'(\xi), \chi_2{}' = \frac{B^*\left[2(\chi_1)^2 + \chi_2(\chi_5 + m(\xi+\alpha)\varepsilon\chi_1) - (\chi_3)^2\right]}{A^*(1+r^*)^{2m}(\mathrm{Re})^{1-n/1+n}}, \\
\chi_3 = g(\xi), \chi_4 = g'(\xi), \chi_4{}' = \frac{B^*[2\chi_1\chi_3 + \chi_4(\chi_5 + m(\xi+\alpha)\varepsilon\chi_1) - \chi_5\chi_2]}{A^*(1+r^*)^{2m}(\mathrm{Re})^{1-n/1+n}}, \\
\chi_5 = j(\xi), \chi_5{}' = -\left[-2\chi_1 + m(\xi+\alpha)\varepsilon(\chi_2)^2\right], \chi_6 = \theta(\xi), \chi_7 = \theta'(\xi), \\
\chi_7{}' = \frac{D^*(\gamma Pr)^*\left[\chi_5\chi_6\chi_5{}' + \chi_7\begin{pmatrix} m(m-1)(\xi+\alpha)(\varepsilon\chi_1)^2 + m\varepsilon\chi_5\chi_1 + m \\ (\xi+\alpha)\varepsilon(\chi_1)^2 m^2(\xi+\alpha)^2\varepsilon^2\chi_1\chi_2 + m \\ (\xi+\alpha)\varepsilon\chi_5\chi_2 + m(\xi+\alpha)\varepsilon\chi_1\chi_5{}' - m\varepsilon\chi_1\chi_5 \end{pmatrix}\right] - m(\xi+\alpha)\varepsilon\chi_1\chi_7 + \chi_5\chi_7}{C^*C_1^*(1+r^*)^{2m}(\mathrm{Re})^{1-n/1+n}\left[(\chi_5)^2 + m^2(\xi+\alpha)^2\varepsilon^2(\chi_1)^2\right]}, \\
\chi_9{}' = \frac{1/Scd_1\chi_8 + \chi_9\left(-1/Scma\varepsilon\xi(R_0+1)\chi_1 - 1/Scma^2\varepsilon(R_0+1)\chi_1 + 1/Sc(1+r^*)^{-m}a\chi_3\right)}{\alpha^2(1+r^*)^{-2m}}, \\
\chi_1(0) = 0, \chi_3(0) = 1, C^*C_1^*\left[(1+r^*)^{2m}\mathrm{Re}^{1-n/1+n}\mathrm{Me}\right]\chi_7 + D^*\mathrm{Pr}^*\chi_{5,}\chi_6 = 1, \\
\chi_1(\infty), \chi_3(\infty), \chi_6(\infty), \chi_8(\infty).
\end{gathered} \tag{25}
$$

Step 2: introducing parameter p

$$
\begin{gathered}
\chi_1 = f(\xi), \chi_2 = f'(\xi), \\
\chi_2{}' = \frac{B^*\left[2(\chi_1)^2 + (\chi_2 - 1)p(\chi_5 + m(\xi+\alpha)\varepsilon\chi_1) - (\chi_3)^2\right]}{A^*(1+r^*)^{2m}(\mathrm{Re})^{1-n/1+n}}, \\
\chi_3 = g(\xi), \chi_4 = g'(\xi), \\
\chi_4{}' = \frac{B^*[2\chi_1\chi_3 + (\chi_4 - 1)p(\chi_5 + m(\xi+\alpha)\varepsilon\chi_1) - \chi_5\chi_2]}{A^*(1+r^*)^{2m}(\mathrm{Re})^{1-n/1+n}}, \\
\chi_5 = j(\xi), \chi_5{}' = -\left[-2\chi_1 + (\chi_5 - 1)p - \chi_5 + m(\xi+\alpha)\varepsilon(\chi_2)^2\right], \\
\chi_6 = \theta(\xi), \chi_7 = \theta'(\xi), \\
\chi_7{}' = \frac{D^*(\gamma Pr)^*\left[\chi_5\chi_6\chi_5{}' + (\chi_7 - 1)p\begin{pmatrix} m(m-1)(\xi+\alpha)(\varepsilon\chi_1)^2 + m\varepsilon\chi_5 \\ \chi_1 + (\xi+\alpha)m\varepsilon(\chi_1)^2 + m^2(\xi+\alpha)^2\varepsilon^2\chi_1\chi_2 + (\xi+\alpha)m\varepsilon\chi_5\chi_2 + \\ m(\xi+\alpha)\varepsilon\chi_1\chi_5{}' - m\varepsilon\chi_1\chi_5 \end{pmatrix}\right] - m(\xi+\alpha)\varepsilon\chi_1\chi_7 + \chi_5\chi_7}{C^*C_1^*(1+r^*)^{2m}(\mathrm{Re})^{1-n/1+n}\left[(\chi_5)^2 + m^2(\xi+\alpha)^2\varepsilon^2(\chi_1)^2\right]}, \\
\chi_9{}' = \frac{1/Scd_1\chi_8 + (\chi_9 - 1)p\left(1/Sc - ma\varepsilon\xi(R_0+1)\chi_1 - 1/Scma^2\varepsilon(R_0+1)\chi_1 + 1/Sc(1+r^*)^{-m}a\chi_3\right)}{\alpha^2(1+r^*)^{-2m}}.
\end{gathered} \tag{26}
$$

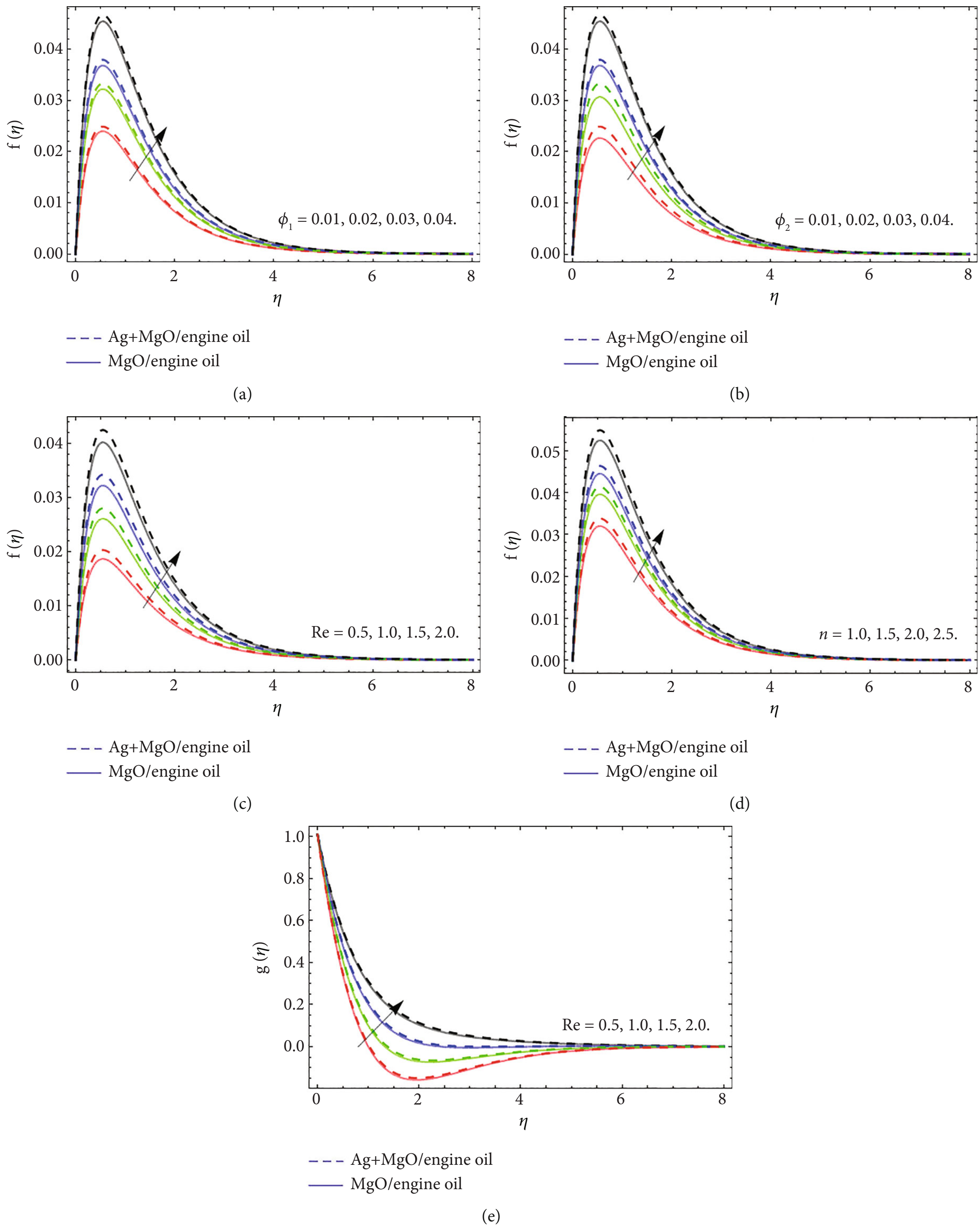

FIGURE 2: The nature of radial velocity $f(\eta)$ and tangential velocity $g(\eta)$ profiles versus (a) volume friction ϕ_1, (b) volume friction ϕ_2, (c) Reynold number Re, (d) power-law exponent n, and (e) Reynold number Re.

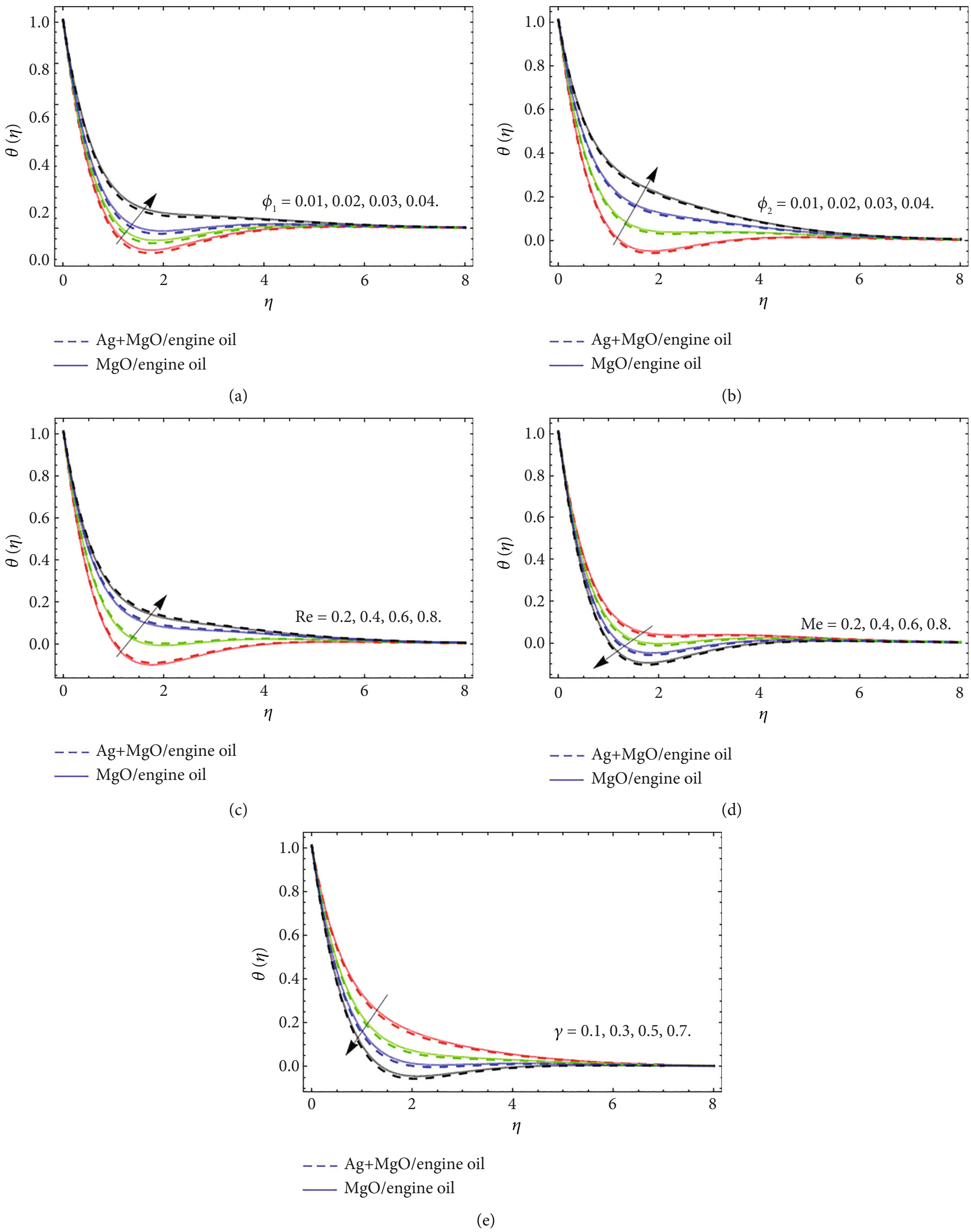

Figure 3: The energy outlines $\theta(\eta)$ versus (a) volume friction ϕ_1, (b) volume friction ϕ_2, (c) Reynold number Re, (d) melting coefficient Me, and (e) thermal relaxation parameter γ, respectively.

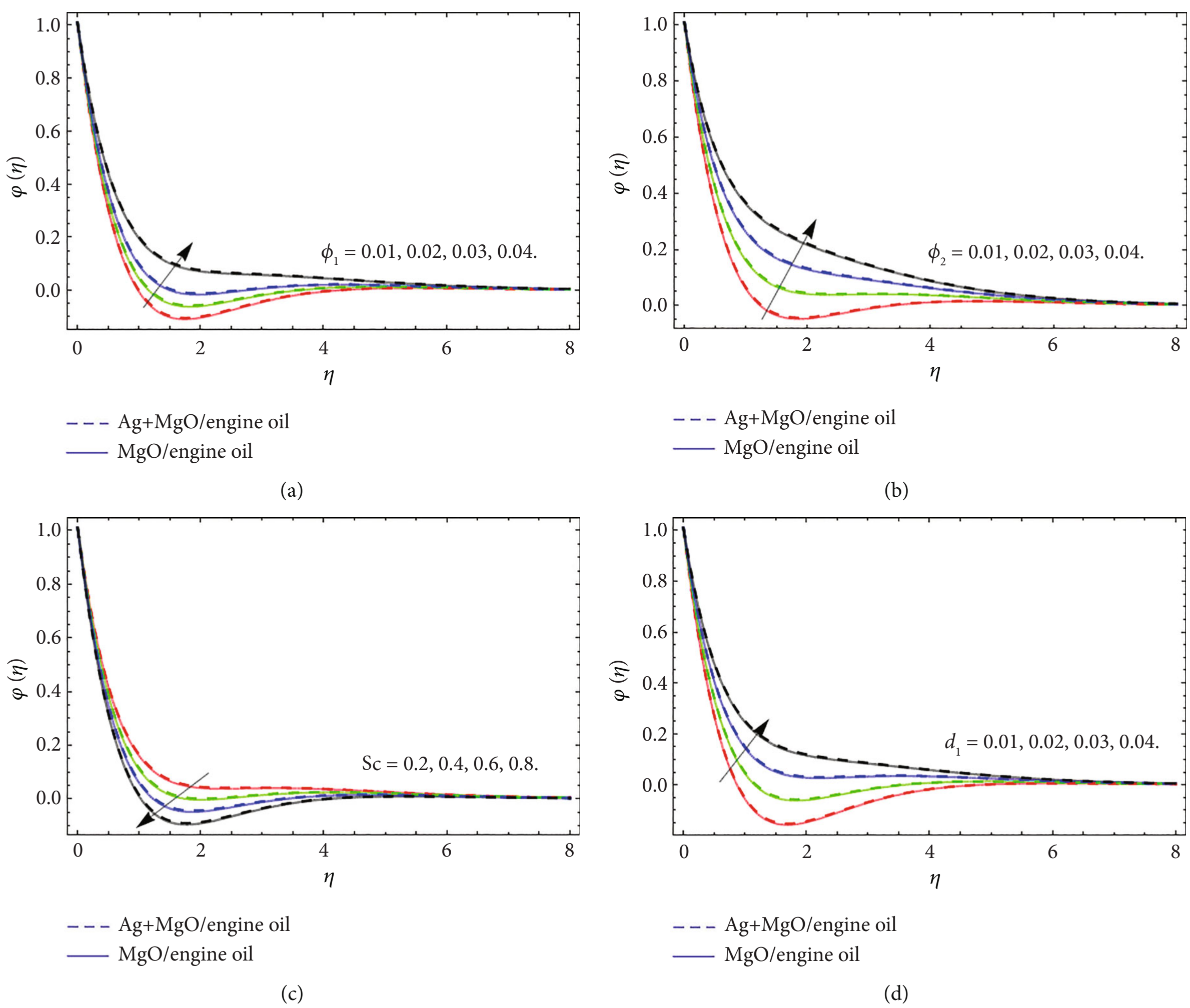

FIGURE 4: The nature of mass transition $\varphi(\eta)$ versus (a) volume friction ϕ_1, (b) volume friction ϕ_2, (c) Schmidt number Sc, (d) chemical reaction d_1, respectively.

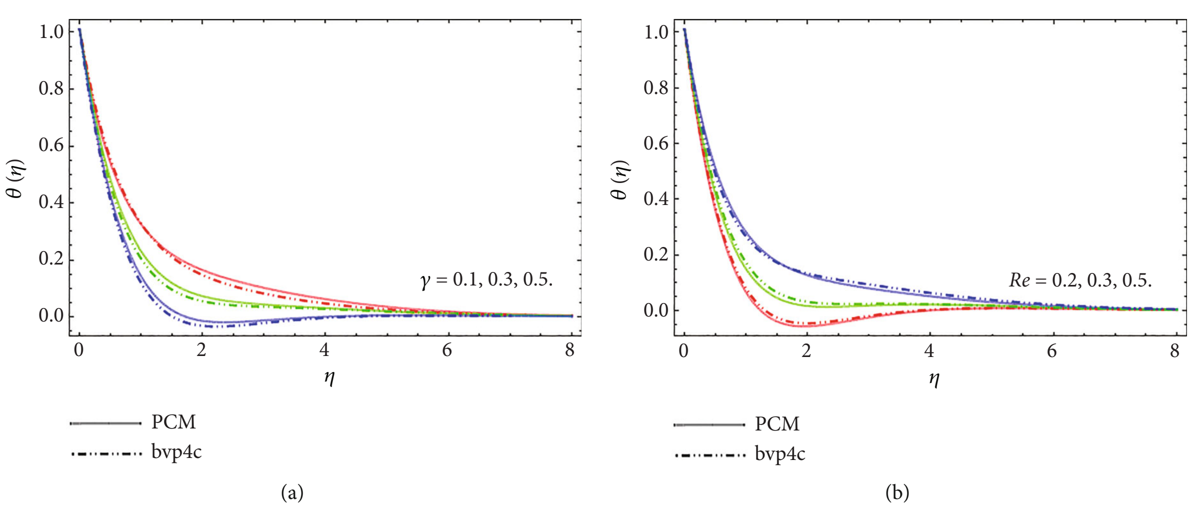

FIGURE 5: The comparison between PCM and Matlab built-in package bvp4c.

Table 2: The experimental values of Ag, MO, and engine oil [47].

	$\rho(\mathrm{kg/m^3})$	$C_p(J/\mathrm{kg}\cdot\mathrm{K})$	$k(\mathrm{W/mK})$
Engine oil	884	1910	0.114
Magnesium oxide	3560	955	45
Silver	10,500	235	429

Table 3: Comparative analysis with the existing literature, when $n = 1$ and $\phi_{hnf} = 0$..

Order of approximations	$f'(0)$	$-g'(0)$
Present work	0.499321	0.500761
Zhang *et al.* [47]	0.497201	0.509623
Xun et al. [50]	0.410221	0.515911
Ming *et al.* [51]	0.410200	0.515901

Table 4: Statistical outcomes for skin friction $(f'(0),-g'(0))$.

m	τ	Re	ϕ_2	$f'(0)$	$-g'(0)$
0.1	0.4	1.0	0.03	0.0474535	0.0702328
0.5	0.4	1.0	0.03	0.0554123	0.0739932
1.0	0.4	1.0	0.03	0.0664852	0.0815843
1.5	0.4	1.0	0.03	0.0791107	0.1130261
1.0	0.1	1.0	0.03	0.0664588	0.0817175
1.0	0.3	1.0	0.03	0.0664760	0.0716306
1.0	0.7	1.0	0.03	0.0664968	0.0815362
1.0	0.4	1.0	0.03	0.0665151	0.0814336
1.0	0.4	0.1	0.03	0.0629418	0.1161421
1.0	0.4	0.5	0.03	0.0685427	0.0857223
1.0	0.4	1.5	0.03	0.0656935	0.0792518
1.0	0.4	2.5	0.00	0.0644128	0.0764015
1.0	0.4	1.0	0.01	0.0726520	0.1136461
1.0	0.4	1.0	0.02	0.0705745	0.0893014
1.0	0.4	1.0	0.03	0.0686036	0.0852958
1.0	0.4	1.0	0.04	0.0667325	0.0815843

Step 3: apply the Cauchy principle and discretized Equation (26)

$$\frac{U^{i+1} - U^i}{\Delta\eta} = AU^{i+1}, \quad \frac{W^{i+1} - W^i}{\Delta\eta} = AW^{i+1}. \tag{27}$$

Finally, we get the iterative form as

$$U^{i+1} = (I - \Delta\eta A)^{-1} U^i, \; W^{i+1} = (I - \Delta\eta A)^{-1}\left(W^i + \Delta\eta R\right). \tag{28}$$

4. Results and Discussion

The discussion segment analyzed the comportment of velocity, energy, and mass-circulation as compared to the deviation of numerous physical parameters for hybrid nanoliquid consisting of Ag and magnetic nanoparticles.

Table 5: Arithmetic results for Nusselt number $(k_{nf}/k_f\theta'(0), k_{hnf}/k_f\theta'(0))$.

Parameters Me	Re	ϕ_1, ϕ_2	PCM $(k_{nf}/k_f)\theta'(0)$	PCM $(k_{hnf}/k_f)\theta'(0)$	bvp4c $(k_{hnf}/k_f)\theta'(0)$
0.1			0.0474535	0.0484531	0.0484340
0.5			0.0354123	0.0366122	0.0366031
1.0			0.0364852	0.0369853	0.0369542
1.5			0.0291107	0.0271407	0.0271268
	0.2		0.0564588	0.0554555	0.0554463
	0.3		0.0574760	0.0575961	0.0575870
	0.4		0.0578962	0.0589965	0.0589834
		0.01	0.0673420	0.0683460	0.0683352
		0.02	0.0683241	0.0693271	0.0693160
		0.03	0.0690324	0.0713142	0.0713021
		0.04	0.0723419	0.0743319	0.0743237

Table 6: Numerical outcomes for Sherwood number.

Sc	d_1	ϕ_1, ϕ_2	$(D_{nf}/D_f)\varphi'(0)$	$(D_{hnf}/D_f)\varphi'(0)$
0.2			0.0632328	0.0642322
0.4			0.062932	0.0639336
0.6			0.0615843	0.0614845
0.8			0.5930261	0.5910240
	0.1		0.0714336	0.0734331
	0.2		0.0761427	0.0771426
	0.3		0.0817223	0.0867224
	0.4		0.0822516	0.0882513
		0.01	0.0627612	0.0677635
		0.02	0.0638732	0.0728754
		0.03	0.6687450	0.7774504
		0.04	0.7026718	0.7906714

The default values used while solving the set of 1st order ODEs through PCM code are $\phi_1 = \phi_2 = 0.01$, $\mathrm{Re} = 0.5$, $n = 1.0$, $\mathrm{Me} = 0.2$, $\gamma = 0.1$, $Sc = 0.2$, $d_1 = 0.01$ and $\tau = 0.4$.

4.1. Velocity Profile. Figures 2(a)–2(e) expose the nature of radial velocity $f(\eta)$ and tangential velocity $g(\eta)$ profiles versus volume friction ϕ_1, volume friction ϕ_2, Reynold number Re, power-law exponent n, and Reynold number Re. Figures 2(a) and 2(b) particularize that the velocity field rises with the growing values of volume friction of both silver and magnetic nanoparticulates. Physically, the specific heat capacity of engine oil is much higher than silver and magnesium compounds that is why the increasing quantity of such nanomaterials reduces the average heat capacity of HNF and causes the elevation of fluid velocity. Figures 2(c) and 2(e) display the dominance of both radial $f(\eta)$ and tangential velocity $g(\eta)$ profiles against Reynold number Re. The upshot of Reynold's number increases the rotation of the disk, which accelerates the fluid particles and exercises their kinetic energy, which causes the improvement in the velocity field. Similar behavior of radial velocity has been observed versus the increment of power-law exponent n in Figure 2 (d). The positive variation in the power-law exponent significantly enhances the fluid velocity in the radial direction.

4.2. Energy Distribution Profile. Figures 3(a)–3(e) illuminate the nature of energy transition $\theta(\eta)$ versus volume friction ϕ_1, volume friction ϕ_2, Reynold number Re, melting coefficient, and thermal relaxation parameter $\gamma_,$ respectively. As discussed in Figure 2, the specific heat capacity of engine oil is much higher than silver and magnesium compounds that is why the increasing quantity of such nanomaterials reduces the average heat capacity of hybrid nanofluid and causes a rise in internal heat, which encourage both velocity and energy transmission rate. Figure 3(c) reports the Reynold number upshot on the energy profile. The number of rotations enhances with the variation of Reynold number that is why due to internal kinetic energy fluid temperature $\theta(\eta)$ also enhances. The effect of both melting coefficient and thermal relaxation term γ reduces energy contour as shown in Figures 3(d) and 3(e). The specific heat capacity of fluid improves with the flourishing values of melting coefficient, as a result, energy transference enhances.

4.3. Mass Transfer Profile. Figures 4(a)–4(d) spot the nature of mass transition $\varphi(\eta)$ versus volume friction ϕ_1, volume friction ϕ_2, Schmidt number Sc, and chemical reaction d_1, respectively. Mass transmission enhances with the rising quantity of nanoparticles, because, as we have discussed earlier, the rising values of volume friction parameters ϕ_1 and ϕ_2 significantly elevated the heat and fluid velocity that is why the mass transition also enhances their effects as shown in Figures 4(a) and 4(b). The upshot of the Schmidt number boosts the fluid kinetic viscosity, which results in the reduction of concentration profile $\varphi(\eta)$ as illustrated in Figure 4(c). The energy transport rate is reduced by the chemical reaction variable, while the mass transport rate is increased. An increase in the intensity of$d_1$indicates that the species concentration interaction is less with the thermal boundary layer and more with the momentum Figure 4(d).

Figure 5 reports the comparative assessment of PCM technique with Matlab code bvp4c. From Figures 5(a) and 5(b), it can be clearly observed that both techniques show best settlement and PCM procedure is a reliable method. Table 2 describes the experimental values of Ag, MgO, and engine oil. Table 3 displays the comparative analysis of the current work with the existing literature, in which the present work revealed the best settlement with them. Table 4 presents the numerical results for skin friction. It has been observed that the drag force enhances along both radial and tangential direction with the variation of parameter m and τ while reduces the effect of Reynold number. Table 5 communicates the numerical outcomes for Nusselt number versus melting coefficient, Reynold number, and both nanofluid and hybrid nanofluid. As comparative to the simple nanofluid, hybrid nanofluid energy transition rate is faster against volume friction coefficient ϕ_1, ϕ_2, respectively. Table 6 displays the Sherwood number versus volume friction parameter ϕ_1, ϕ_2, Schmidt number, and chemical reaction d_1 constant, respectively. The mass transference rate diminishes with the rising effect of Schmidt number while enhances against the increasing quantity of chemical reaction parameter and volume friction constants.

5. Conclusion

The 3D flow of Ag and MgO HNF past over a gyrating disk of varying thickness has been reported in the present estimation. The hybrid nanoliquid is synthesized by using silver, magnetic nanoparticulate, and engine oil. The energy transition consequences are examined in the involvement of melting heat propagation. The highly nonlinear system of PDEs is processed through the proper similarity conversions to attain the coupled ODE system. The obtained system of modeled equations is numerically solved through the PCM technique. The key points are rebound as follows:

(i) The radial $f(\eta)$ and tangential $g(\eta)$ velocities and energy propagation enhance with the rising values of volume friction of both silver $\phi_{1=Ag}$ and magnetic nanoparticulates $\phi_{2=MgO}$

(ii) The upshot of Reynold number Re improves the velocity and energy transition of fluid flow, due to an increase in the number of disk's rotation

(iii) The positive variation in power-law exponent n significantly enhances the fluid velocity in the radial direction

(iv) The increasing quantity of nanomaterials reduces the average heat capacity of hybrid nanofluid and causes a rise in internal heat, which encourages both velocity and heat transition rate

(v) The effect of both melting coefficient and thermal relaxation term γ reduces fluid temperature

Data Availability

The relevant data exist in the manuscript.

Conflicts of Interest

The authors declare that they have no conflicts of interest.

Authors' Contributions

Muhammad Bilal and Taza Gul contributed to the modeling and writing manuscript and conception or design of the work. Abir Mouldi, Safyan Mukhtar, Wajdi Alghamdi, Souhail Mohamed Bouzgarrou, and Nosheen Feroz contributed to the validation and critical revision of the article.

Acknowledgments

The authors extend their appreciation to the Deanship of Scientific Research at King Khalid University for funding this work through Large Groups Project under grant number (RGP2./14/43).

References

[1] A. Ahmadian, M. Bilal, M. A. Khan, and M. I. Asjad, "The non-Newtonian Maxwell nanofluid flow between two parallel rotating disks under the effects of magnetic field," *Scientific Reports*, vol. 10, no. 1, pp. 1–14, 2020.

[2] K. Anantha Kumar, V. Sugunamma, and N. Sandeep, "Influence of viscous dissipation on MHD flow of micropolar fluid over a slendering stretching surface with modified heat flux model," *Journal of Thermal Analysis and Calorimetry*, vol. 139, no. 6, pp. 3661–3674, 2020.

[3] B. Ramadevi, K. Anantha Kumar, V. Sugunamma, J. V. Ramana Reddy, and N. Sandeep, "Magnetohydrodynamic mixed convective flow of micropolar fluid past a stretching surface using modified Fourier's heat flux model," *Journal of Thermal Analysis and Calorimetry*, vol. 139, no. 2, pp. 1379–1393, 2020.

[4] Y. P. Lv, E. A. Algehyne, M. G. Alshehri et al., "Numerical approach towards gyrotactic microorganisms hybrid nanoliquid flow with the hall current and magnetic field over a spinning disk," *Scientific Reports*, vol. 11, no. 1, pp. 1–13, 2021.

[5] Y. X. Li, T. Muhammad, M. Bilal, M. A. Khan, A. Ahmadian, and B. A. Pansera, "Fractional simulation for Darcy-Forchheimer hybrid nanoliquid flow with partial slip over a spinning disk," *Alexandria Engineering Journal*, vol. 60, no. 5, pp. 4787–4796, 2021.

[6] M. Khan, J. Ahmed, and W. Ali, "Thermal analysis for radiative flow of magnetized Maxwell fluid over a vertically moving rotating disk," *Journal of Thermal Analysis and Calorimetry*, vol. 143, no. 6, pp. 4081–4094, 2021.

[7] M. Shuaib, R. A. Shah, and M. Bilal, "Von-Karman rotating flow in variable magnetic field with variable physical properties," *Advances in Mechanical Engineering*, vol. 13, no. 2, 2021.

[8] M. Bilal, A. Saeed, T. Gul, I. Ali, W. Kumam, and P. Kumam, "Numerical approximation of microorganisms hybrid nanofluid flow induced by a wavy fluctuating spinning disc," *Coatings*, vol. 11, no. 9, p. 1032, 2021.

[9] A. Hafeez, M. Khan, and J. Ahmed, "Thermal aspects of chemically reactive Oldroyd-B fluid flow over a rotating disk with Cattaneo–Christov heat flux theory," *Journal of Thermal Analysis and Calorimetry*, vol. 144, no. 3, pp. 793–803, 2021.

[10] H. Waqas, M. Imran, T. Muhammad, S. M. Sait, and R. Ellahi, "Numerical investigation on bioconvection flow of Oldroyd-B nanofluid with nonlinear thermal radiation and motile microorganisms over rotating disk," *Journal of Thermal Analysis & Calorimetry*, vol. 145, no. 2, pp. 523–539, 2021.

[11] A. Tassaddiq, S. Khan, M. Bilal et al., "Heat and mass transfer together with hybrid nanofluid flow over a rotating disk," *AIP Advances*, vol. 10, no. 5, article 055317, 2020.

[12] I. Tlili, N. Sandeep, M. G. Reddy, and H. A. Nabwey, "Effect of radiation on engine oil-TC4/NiCr mixture nanofluid flow over a revolving cone in mutable permeable medium," *Ain Shams Engineering Journal*, vol. 11, no. 4, pp. 1255–1263, 2020.

[13] F. Jamil and H. M. Ali, "Applications of hybrid nanofluids in different fields," in *In Hybrid nanofluids for convection heat transfer*, Academic Press, 2020.

[14] G. P. Ashwinkumar, S. P. Samrat, and N. Sandeep, "Convective heat transfer in MHD hybrid nanofluid flow over two different geometries," *International Communications in Heat and Mass Transfer*, vol. 127, p. 105563, 2021.

[15] N. Joshi, A. K. Pandey, H. Upreti, and M. Kumar, "Mixed convection flow of magnetic hybrid nanofluid over a bidirectional porous surface with internal heat generation and a higher-order chemical reaction," *Heat Transfer*, vol. 50, no. 4, pp. 3661–3682, 2021.

[16] H. Upreti, A. K. Pandey, and M. Kumar, "Thermophoresis and suction/injection roles on free convective MHD flow of Ag–kerosene oil nanofluid," *Journal of Computational Design and Engineering*, vol. 7, no. 3, pp. 386–396, 2020.

[17] Y. M. Chu, U. Nazir, M. Sohail, M. M. Selim, and J. R. Lee, "Enhancement in thermal energy and solute particles using hybrid nanoparticles by engaging activation energy and chemical reaction over a parabolic surface via finite element approach," *Fractal and Fractional*, vol. 5, no. 3, p. 119, 2021.

[18] C. Fisher, E. Rider, Z. Jun Han, S. Kumar, I. Levchenko, and K. K. Ostrikov, "Applications and nanotoxicity of carbon nanotubes and graphene in biomedicine," *Journal of Nanomaterials*, vol. 2012, 19 pages, 2012.

[19] M. I. Asjad, M. Zahid, Y. M. Chu, and D. Baleanu, "Prabhakar fractional derivative and its applications in the transport phenomena containing nanoparticles," *Thermal Science*, vol. 25, no. 2, pp. 411–416, 2021.

[20] K. Singh, A. K. Pandey, and M. Kumar, "Slip flow of micropolar fluid through a permeable wedge due to the effects of chemical reaction and heat source/sink with Hall and ion-slip currents: an analytic approach," *Propulsion and Power Research*, vol. 9, no. 3, pp. 289–303, 2020.

[21] I. Ullah, "Heat transfer enhancement in Marangoni convection and nonlinear radiative flow of gasoline oil conveying boehmite alumina and aluminum alloy nanoparticles," *International Communications in Heat and Mass Transfer*, vol. 132, p. 105920, 2022.

[22] X. Wang, L. Luo, J. Xiang et al., "A comprehensive review on the application of nanofluid in heat pipe based on the machine learning: theory, application and prediction," *Renewable and Sustainable Energy Reviews*, vol. 150, p. 111434, 2021.

[23] A. U. Khan, A. U. Khan, B. Li et al., "Biosynthesis of silver capped magnesium oxide nanocomposite using _Olea cuspidata_ leaf extract and their photocatalytic, antioxidant and antibacterial activity," *Photodiagnosis and Photodynamic Therapy*, vol. 33, p. 102153, 2021.

[24] I. Ullah, "Activation energy with exothermic/endothermic reaction and Coriolis force effects on magnetized nanomaterials flow through Darcy–Forchheimer porous space with variable features," *Waves in Random and Complex Media*, vol. 2022, pp. 1–15, 2022.

[25] H. Upreti, A. K. Pandey, and M. Kumar, "Assessment of entropy generation and heat transfer in three-dimensional hybrid nanofluids flow due to convective surface and base fluids," *Journal of Porous Media*, vol. 24, no. 3, pp. 35–50, 2021.

[26] I. Ullah, R. Ullah, M. S. Alqarni, W. F. Xia, and T. Muhammad, "Combined heat source and zero mass flux features on magnetized nanofluid flow by radial disk with the applications of Coriolis force and activation energy," *International Communications in Heat and Mass Transfer*, vol. 126, p. 105416, 2021.

[27] A. Ahmadian, M. Bilal, M. A. Khan, and M. I. Asjad, "Numerical analysis of thermal conductive hybrid nanofluid flow over the surface of a wavy spinning disk," *Scientific Reports*, vol. 10, no. 1, pp. 1–13, 2020.

[28] E. A. Algehyne, M. Areshi, A. Saeed, M. Bilal, W. Kumam, and P. Kumam, "Numerical simulation of bioconvective Darcy Forchhemier nanofluid flow with energy transition over a permeable vertical plate," *Scientific Reports*, vol. 12, no. 1, pp. 1–12, 2022.

[29] X. H. Zhang, A. Algehyne, M. Alshehri, M. Bilal, M. A. Khan, and T. Muhammad, “The parametric study of hybrid nanofluid flow with heat transition characteristics over a fluctuating spinning disk,” *PLoS One*, vol. 16, no. 8, article e0254457, 2021.

[30] N. S. Anuar, N. Bachok, and I. Pop, “Influence of buoyancy force on Ag-MgO/water hybrid nanofluid flow in an inclined permeable stretching/shrinking sheet,” *International Communications in Heat and Mass Transfer*, vol. 123, p. 105236, 2021.

[31] K. Gangadhar, R. E. Nayak, M. V. S. Rao, and T. Kannan, “Nodal/saddle stagnation point slip flow of an aqueous convectional magnesium oxide–gold hybrid nanofluid with viscous dissipation,” *Arabian Journal for Science and Engineering*, vol. 46, no. 3, pp. 2701–2710, 2021.

[32] B. Hiba, F. Redouane, W. Jamshed et al., “A novel case study of thermal and streamline analysis in a grooved enclosure filled with (Ag–MgO/Water) hybrid nanofluid: Galerkin FEM,” *Case Studies in Thermal Engineering*, vol. 28, p. 101372, 2021.

[33] K. Singh, A. K. Pandey, and M. Kumar, “Melting heat transfer assessment on magnetic nanofluid flow past a porous stretching cylinder,” *Journal of the Egyptian Mathematical Society*, vol. 29, no. 1, pp. 1–14, 2021.

[34] S. Rashid, S. Sultana, Y. Karaca, A. Khalid, and Y. M. Chu, “Some further extensions considering discrete proportional fractional operators,” *Fractals*, vol. 30, no. 1, p. 2240026, 2022.

[35] N. Joshi, H. Upreti, A. K. Pandey, and M. Kumar, “Heat and mass transfer assessment of magnetic hybrid nanofluid flow via bidirectional porous surface with volumetric heat generation,” *International Journal of Applied and Computational Mathematics*, vol. 7, no. 3, pp. 1–17, 2021.

[36] N. Joshi, H. Upreti, and A. K. Pandey, “MHD Darcy-Forchheimer Cu-Ag/H2O-C2H6O2 hybrid nanofluid flow via a porous stretching sheet with suction/blowing and viscous dissipation,” *International Journal For Computational Methods In Engineering Science And Mechanics*, vol. 2022, pp. 1–9, 2022.

[37] K. Karthikeyan, P. Karthikeyan, H. M. Baskonus, K. Venkatachalam, and Y. M. Chu, “Almost sectorial operators on Ψ-Hilfer derivative fractional impulsive integro-differential equations,” *Mathematical Methods in the Applied Sciences*, vol. 2022, 2021.

[38] M. A. Abd El Salam, M. A. Ramadan, M. A. Nassar, P. Agarwal, and Y. M. Chu, “Matrix computational collocation approach based on rational Chebyshev functions for nonlinear differential equations,” *Advances in Difference Equations*, vol. 2021, 17 pages, 2021.

[39] Y. M. Chu, N. A. Shah, P. Agarwal, and J. D. Chung, “Analysis of fractional multi-dimensional Navier–Stokes equation,” *Advances in Difference Equations*, vol. 2021, 18 pages, 2021.

[40] X. Qiang, A. Mahboob, and Y. M. Chu, “Numerical approximation of fractional-order Volterra integrodifferential equation,” *Journal of Function Spaces*, vol. 2020, 12 pages, 2020.

[41] A. Patil, *A Modification and Application of Parametric Continuation Method to Variety of Nonlinear Boundary Value Problems in Applied Mechanics*, Rochester Institute of Technology, 2016.

[42] M. Shuaib, R. A. Shah, and M. Bilal, “Variable thickness flow over a rotating disk under the influence of variable magnetic field: an application to parametric continuation method,” *Advances in Mechanical Engineering*, vol. 12, no. 6, 2020.

[43] M. Shuaib, R. A. Shah, I. Durrani, and M. Bilal, “Electrokinetic viscous rotating disk flow of Poisson-Nernst-Planck equation for ion transport,” *Journal of Molecular Liquids*, vol. 313, p. 113412, 2020.

[44] Z. Dombovari, A. Iglesias, T. G. Molnar et al., “Experimental observations on unsafe zones in milling processes,” *Philosophical Transactions of the Royal Society A*, vol. 377, no. 2153, p. 20180125, 2019.

[45] Y. M. Chu, U. Khan, A. Zaib, S. H. A. M. Shah, and M. Marin, “Numerical and computer simulations of cross-flow in the streamwise direction through a moving surface comprising the significant impacts of viscous dissipation and magnetic fields: stability analysis and dual solutions,” *Mathematical Problems in Engineering*, vol. 2020, 11 pages, 2020.

[46] S. B. Chen, H. Jahanshahi, O. A. Abba et al., “The effect of market confidence on a financial system from the perspective of fractional calculus: numerical investigation and circuit realization,” *Chaos, Solitons & Fractals*, vol. 140, p. 110223, 2020.

[47] Y. Zhang, N. Shahmir, M. Ramzan, H. Alotaibi, and H. M. Aljohani, “Upshot of melting heat transfer in a Von Karman rotating flow of gold- silver/engine oil hybrid nanofluid with Cattaneo-Christov heat flux,” *Case Studies in Thermal Engineering*, vol. 26, p. 101149, 2021.

[48] G. Taza and M. Zakaullah, “A thermal performance of the graphene oxide nanofluids flow in an upright channel through a permeable medium,” *IEEE Access*, vol. 7, pp. 102345–102355, 2019.

[49] T. Hayat, S. Qayyum, M. Imtiaz, and A. Alsaedi, “MHD flow and heat transfer between coaxial rotating stretchable disks in a thermally stratified medium,” *PLoS One*, vol. 11, no. 5, article e0155899, 2016.

[50] S. Xun, J. Zhao, L. Zheng, X. Chen, and X. Zhang, “Flow and heat transfer of Ostwald-de Waele fluid over a variable thickness rotating disk with index decreasing,” *International Journal of Heat and Mass Transfer*, vol. 103, pp. 1214–1224, 2016.

[51] C. Ming, L. Zheng, and X. Zhang, “Steady flow and heat transfer of the power-law fluid over a rotating disk,” *International Communications in Heat and Mass Transfer*, vol. 38, no. 3, pp. 280–284, 2011.